

Methods

PDEAAm synthesis

PDEAAm was prepared by group transfer polymerization⁹ to ensure a narrow molecular-mass distribution. Tetrabutylammonium acetate was used as the catalyst and 1-methoxyl-1-(trimethylsiloxy)-2-methyl-1-propene as the initiator. In the final stage of polymerization, a hydroxyl group was incorporated into one end of each polymer chain by adding a capping agent, 2-(trimethylsiloxy)ethyl methacrylate. The trimethylsiloxy group was subsequently removed by hydrolysis, to generate the –OH end group. The hydroxyl end group was subsequently derivatized to a vinyl sulphone group by reacting with divinyl sulphone^{6,7}. The molecular mass and polydispersity of the polymer were determined in tetrahydrofuran, using gel permeation chromatography calibrated with polystyrene molecular-mass standards. All of the polymers have a molecular-mass polydispersity of less than 1.2.

Conjugation

Conjugation of PDEAAm to E51K/N118K streptavidin was performed at pH 9.5, 4 °C for 16 h. Three thermally induced precipitations of the conjugate were conducted to remove any unconjugated E51K/N118K streptavidin, which remained in the supernatant. Iminobiotin affinity chromatography was employed to separate the conjugate from the unreacted free polymer¹⁰. The purified streptavidin–PDEAAm conjugate was then immobilized on magnetic microbeads for the biotinylated-protein binding assays.

Binding assays

The conjugates and, as a control, the unconjugated E51K/N118K streptavidin were immobilized on magnetic microbeads and suspended in 100 mM sodium phosphate buffer, pH 8, containing 0.2 wt% of BSA. The suspensions were incubated in a 10 °C water bath for 1 h before addition of the biotinylated protein. They were mixed and then further incubated at 10 °C for 30 min to reach binding equilibrium. The magnetic beads were separated and the fluorescence intensities (excitation wavelength, 494 nm; emission wavelength, 520 nm) of the supernatant were measured versus control solutions without magnetic microbeads. The solutions were then incubated at a higher temperature and the same operations were repeated. One nmol of either E51K/N118K–PDEAAm conjugate or E51K/N118K was used for each assay.

Determination of LCST

The LCST of the E51K/N118K–PDEAAm-12.8k conjugate was determined in 100 mM sodium phosphate buffer, pH 8.0, containing 0.2 wt% of BSA, by measuring absorbance at 500 nm versus temperature. The LCST is defined as the temperature where the light absorbance is 10% of the maximum value.

Synthesis of biotinylated PDEAAm

A primary amino group at the end of the PDEAAm chain was reacted with sulph-NHS-LC-biotin (from Pierce). B-PDEAAm was then complexed to E51K/N118K streptavidin, which was immobilized on magnetic beads via the interaction of biotin and streptavidin.

Received 29 December 2000; accepted 12 February 2001.

1. Fong, R. B., Ding, Z., Long, C. J., Hoffman, A. S. & Stayton, P. S. Thermoprecipitation of streptavidin via oligonucleotide-mediated self-assembly with poly(N-isopropylacrylamide). *Bioconj. Chem.* **10**, 720–725 (1999).
2. Wilchek, M. & Bayer, E. A. *Avidin–Biotin Technology* (Academic, New York, 1990).
3. Schlosser, M., Hahmann, J., Ziegler, B., Augstein, P. & Ziegler, M. Sensitive monoclonal antibody-based sandwich ELISA for determination of the diabetes-associated autoantigen glutamic acid decarboxylase GAD65. *J. Immunoass.* **18**, 289–307 (1997).
4. Bloch, B. Biotinylated probes for in situ hybridization histochemistry: Use for mRNA detection. *J. Histochem. Cytochem.* **41**, 1751–1754 (1993).
5. Stayton, P. S. *et al.* Control of protein-ligand recognition using a stimuli-responsive polymer. *Nature* **378**, 472–474 (1995).
6. Bulmus, V., Ding, Z., Long, C. J., Stayton, P. S. & Hoffman, A. S. Design, synthesis and site-specific conjugation of a pH- and temperature-sensitive polymer to streptavidin for pH-controlled binding and triggered release of biotin. *Bioconj. Chem.* **11**, 78–83 (1999).
7. Ding, Z. *et al.* Temperature control of biotin binding and release with a streptavidin-poly(N-isopropylacrylamide) site-specific conjugate. *Bioconj. Chem.* **10**, 395–400 (1999).
8. Wu, C. & Wang, X. H. Globule-to-coil transition of a single homopolymer chain in solution. *Phys. Rev. Lett.* **80**, 4092–4094 (1998).
9. Sogah, D. Y., Hertler, W. R., Webster, O. W. & Cohen, G. M. Group transfer polymerization. Polymerization of acrylic monomers. *Macromolecules* **20**, 1473–1488 (1987).
10. Hofmann, K., Wood, S. A., Brinton, C. C., Montibeller, J. A. & Finn, F. M. Iminobiotin affinity columns and their application to retrieval of streptavidin. *Proc. Natl Acad. Sci. USA* **77**, 4666–4668 (1980).

Acknowledgements

We thank R. Clark for providing protein G, and N. Murthy for help with PDEAAm synthesis. This work was supported by the National Institutes of Health.

Correspondence and requests for materials should be addressed to A.S.H. (hoffman@u.washington.edu) or P.S.S. (stayton@u.washington.edu).

Evolution of Asian monsoons and phased uplift of the Himalaya–Tibetan plateau since Late Miocene times

An Zhisheng*, John E. Kutzbach†, Warren L. Prell‡ & Stephen C. Porter§

* State Key Laboratory of Loess and Quaternary Geology, Institute of Earth Environment, Chinese Academy of Sciences, Box 17, Xi’an 710054, China
 † Center for Climatic Research, Institute for Environmental Studies, University of Wisconsin–Madison, 1225 W. Dayton Street, Madison, Wisconsin 53706, USA
 ‡ Geological Sciences, Box 1846, Brown University, Providence, Rhode Island 02912-1846, USA
 § Quaternary Research Center, Box 351310, University of Washington, Seattle, Washington 98195, USA

The climates of Asia are affected significantly by the extent and height of the Himalayan mountains and the Tibetan plateau^{1–4}. Uplift of this region began about 50 Myr ago, and further significant increases in altitude of the Tibetan plateau are thought to have occurred about 10–8 Myr ago^{4,5}, or more recently. However, the climatic consequences of this uplift remain unclear. Here we use records of aeolian sediments from China^{6,7} and marine sediments from the Indian^{8–10} and North Pacific oceans¹¹ to identify three stages of evolution of Asian climates: first, enhanced aridity in the Asian interior and onset of the Indian and east Asian monsoons, about 9–8 Myr ago; next, continued intensification of the east Asian summer and winter monsoons, together with increased dust transport to the North Pacific Ocean¹¹, about 3.6–2.6 Myr ago; and last, increased variability and possible weakening of the Indian and east Asian summer monsoons and continued strengthening of the east Asian winter monsoon since about 2.6 Myr ago. The results of a numerical climate-model experiment, using idealized stepwise increases of mountain-plateau elevation, support the argument that the stages in evolution of Asian monsoons are linked to phases of Himalaya–Tibetan plateau uplift and to Northern Hemisphere glaciation.

Continuous sedimentary records of Asian climate are found in China and in marine cores from the Indian and North Pacific oceans (Fig. 1). The planktonic foraminifer *Globigerina bulloides* and upwelling radiolaria from ODP site 722 (Fig. 2) are indices of coastal upwelling in the Arabian Sea and thus of southwesterly wind strength during the Indian summer monsoon^{8,10}. Although carbonate dissolution (often associated with high productivity) reduces the magnitude of the *G. bulloides* index at certain times (Fig. 2), the composite radiolarian and *G. bulloides* records show strengthening of upwelling about 9–8 Myr ago and relatively continuous upwelling thereafter. Magnetic susceptibility flux from ODP site 758 (ref. 9), representing sea-level-mediated fluvial transport from the Ganges and other river systems draining the southern side of the Himalayan–Tibetan orogen, increases about 9 Myr ago. Significantly, new basal dates from the aeolian ‘Red Clay’ sediments on the Chinese Loess plateau (Figs 1, 2) indicate onset of aeolian dust accumulation at about 7.6 Myr ago at Zhaojiachuan (35° 53’ N, 107° 58’ E), 8.0 Myr ago at Chaona (35° 06’ N, 107° 12’ E), and as early as 8.3 Myr ago at Jiaxian (38° 16’ N, 110° 5’ E) (Fang, X.M. and Qiang, X.K., personal communication). Records from North Pacific ODP sites 885 and 886, which accumulated wind-blown dust from Asia, show a major dust peak about 8–7 Myr ago¹¹. The change in oxygen isotope composition of soil carbonates in Pakistan about 9–8 Myr ago¹² (Fig. 2), inferred changes in vegetation from C₃ (forests) to C₄ (grasses) in Pakistan beginning about 8 Myr ago¹³, and a change from mixed needle-leaf and broad-leaf forests to grassland vegetation along the northeastern margin of the Tibetan plateau about 8.5 Myr ago¹⁴, all imply increasing seasonality by about 8 Myr

ago, with most precipitation in summer. These widely distributed observations can be interpreted as signalling an environmental response to a major phase of Himalaya–Tibetan plateau uplift about 9–8 Myr ago. This response is broadly consistent with the climate changes produced in our climate-model experiment. This

experiment used highly idealized stages of elevation history for the Himalayan–Tibetan region; that is, going from relatively small areas with elevations above 1,000 m and maximum elevations between 1,700 and 2,700 m (stages HT-1 and HT-2), with a weak Asian summer monsoon circulation and relatively low summer monsoon

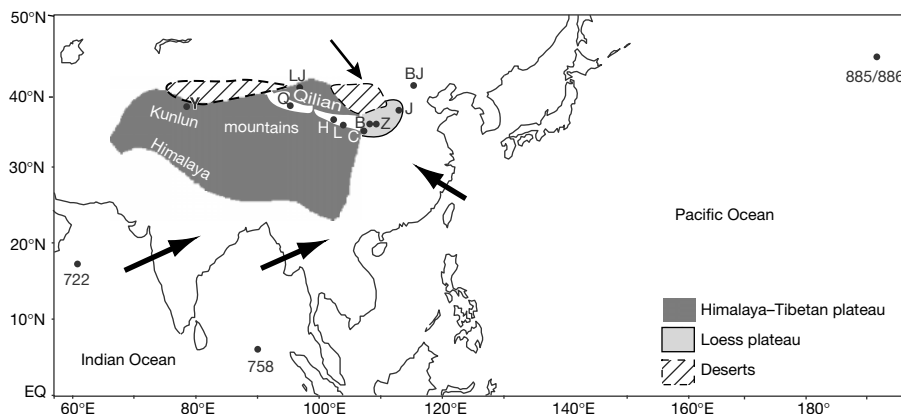


Figure 1 Locations of geographic features and terrestrial and marine records. BJ, Beijing; B, Z and J, locations of the Bajiazui, Zhaojiachuan and Jiaxian sections from the Loess plateau, respectively; C, Chaona site; Y, Ye Cheng site; LJ, Lao Junmiao section; Q and L, the Qaidam and Linxia basins; and H, Haiyuan. The bold arrows (narrow arrow) indicate generalized wind directions of the summer (winter) monsoon.

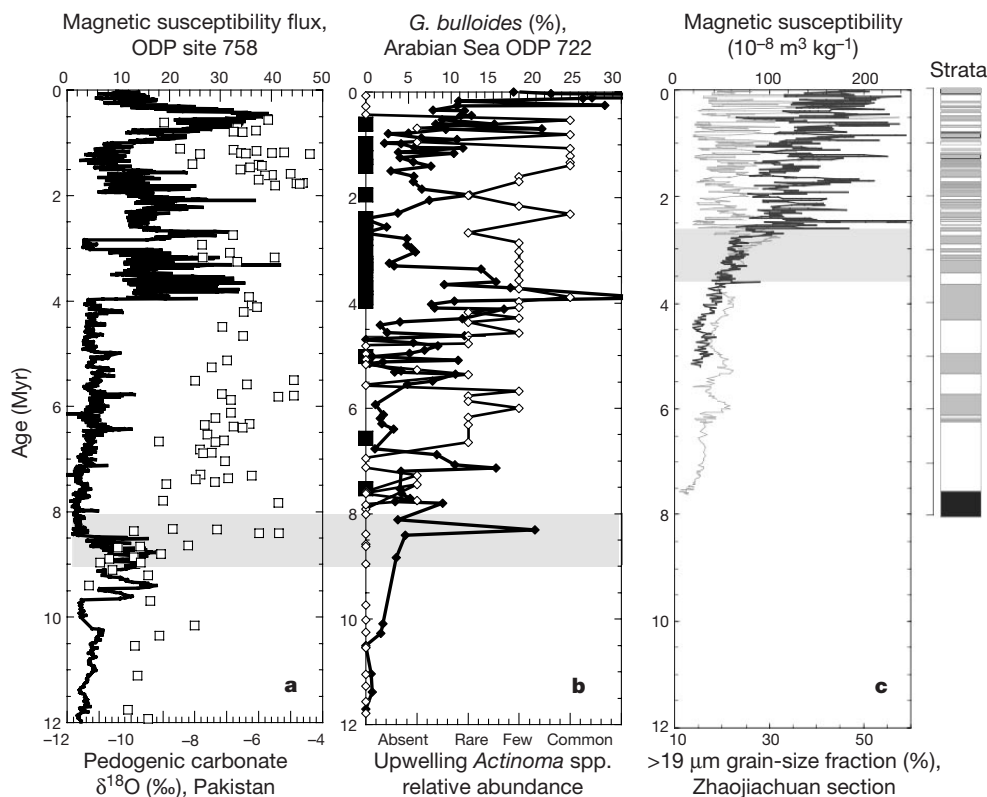


Figure 2 Terrestrial and marine records from the Chinese Loess plateau and the southern margin of Asia. The shaded zones at ~9–8 and 3.6–2.6 Myr ago indicate times of change detailed in the text. **a**, The magnetic susceptibility flux (SI units times sedimentation rate, solid line) from ODP Site 758 (Fig. 1) reflects the sea-level-mediated terrigenous flux to the Bay of Bengal⁹. The $\delta^{18}\text{O}$ of soil carbonates (open squares) in Pakistan¹² reflects increased aridity or a change in the precipitation source about 9–8 Myr ago. The terrestrial record of monsoon influence remains high but variable while the fluvial flux to the Bay of Bengal is low between 8 and 4 Myr ago. This difference is attributed to higher sea level and less transport to the deep sea during the late Miocene. **b**, The abundance of upwelling fauna at ODP Site 722 in the Arabian Sea (Fig. 1). Revised percentage data for planktonic foraminifer *G. bulloides* (filled diamonds) and relative

abundance of radiolarian *Actinoma* spp.⁸ (open diamonds). Intervals of poor carbonate preservation are indicated by filled squares on the time axis. The low *G. bulloides* values from 8–0 Myr ago are mostly attributed to poor carbonate preservation⁸. **c**, The stratigraphy and time series of magnetic susceptibility⁷ (thin line) and >19 μm grain-size fraction (thick line) from the Zhaojiachuan section on the Loess plateau. The chronology is based on the polarity boundary ages^{7,16}, and was obtained by interpolation from a sedimentation model¹⁵ using the >19 μm grain-size fraction and a magnetic susceptibility model⁷ in the basal part where grain-size data are not available. The white, grey, and dark shaded patterns in the simplified stratigraphy column represent loess or loess-like sediment, palaeosols and bedrock, respectively.

precipitation, to a much larger area with elevations above 1,000 m and maximum elevations of 5,700 m (stage HT-3, a stage we associate with the Late Miocene time), with a strong Asian monsoon circulation and increased summer monsoon precipitation (Fig. 3). These changes in continent-scale monsoon circulation are caused primarily by large increases in sensible heating and latent heating (precipitation) that are focused over or along the slopes of the high plateau^{1–4}. In central Asia, precipitation decreases^{2,3} (Fig. 3).

The onset of aeolian deposition in China about 8 Myr ago resulted in long, continuous terrestrial records at Zhaojiachuan and Bajiazui (35° 53' N, 107° 27' E)^{6,7}, within the largest platforms on the Loess plateau (Fig. 1), and in an area that is very sensitive to variations in the east Asian summer and winter monsoons¹⁵. These sequences (Fig. 4) consist of two parts: the upper part corresponds to the well-known loess–palaeosol sequence of Luochuan, aged ≤ 2.6 Myr (ref. 16), which has been correlated with deep-sea sedimentary records; the lower Red Clay sequence consists of inter-layered light-red to reddish-yellow silty loess and light-red to brownish-red palaeosols, and mantles a surface with variable relief and different ages. The quasi-normal grain-size distribution, the 40–60% silt fraction, and other chemical and physical characteristics, indicate an aeolian origin for the sediment^{6,7,17}. Overall southeastward fining of the loessic silt is consistent with north-westerly winter winds. The degree of pedogenesis of the palaeosols, reflected in their colour, texture, and abundance of pedogenic

calcareous nodules, increases southeastward towards regions of increasing summer-monsoon precipitation.

Several indicators of summer and winter monsoon strength have been developed from these loess–palaeosol sequences. The high positive correlation between the frequency-dependent magnetic susceptibility, which can be used to identify ferromagnetic grain size, and the magnetic susceptibility of Red Clay samples indicates that the susceptibility depends mainly on ultra-fine-grained ferromagnetic minerals formed *in situ* during pedogenesis¹⁸. Therefore, susceptibility records in the lower sequence—which have ferromagnetic minerals and magnetic properties similar to those of the overlying loess and palaeosols, and similar susceptibility records to those in the upper sequence—are indices of summer monsoon precipitation¹⁷ (Fig. 4). The overall strong correlation of the magnetic susceptibility series with an independently derived Rb/Sr time-series emphasizes that both indices are measures of summer monsoon strength (Fig. 4). During weathering, Rb is relatively stable, whereas Sr is relatively mobile; therefore, an increased Rb/Sr ratio indicates increased weathering and pedogenesis, and a strong monsoon¹⁹. The coarse-grain fraction and the Al flux (Fig. 4) are indices of winter monsoon strength¹⁵ and the degree of aridity in dust source regions¹¹, respectively.

Based upon the temporal changes of these monsoon indices (Fig. 4), we subdivide the period 6–2 Myr ago into three intervals. The period from 6 to about 3.6 Myr ago shows considerable

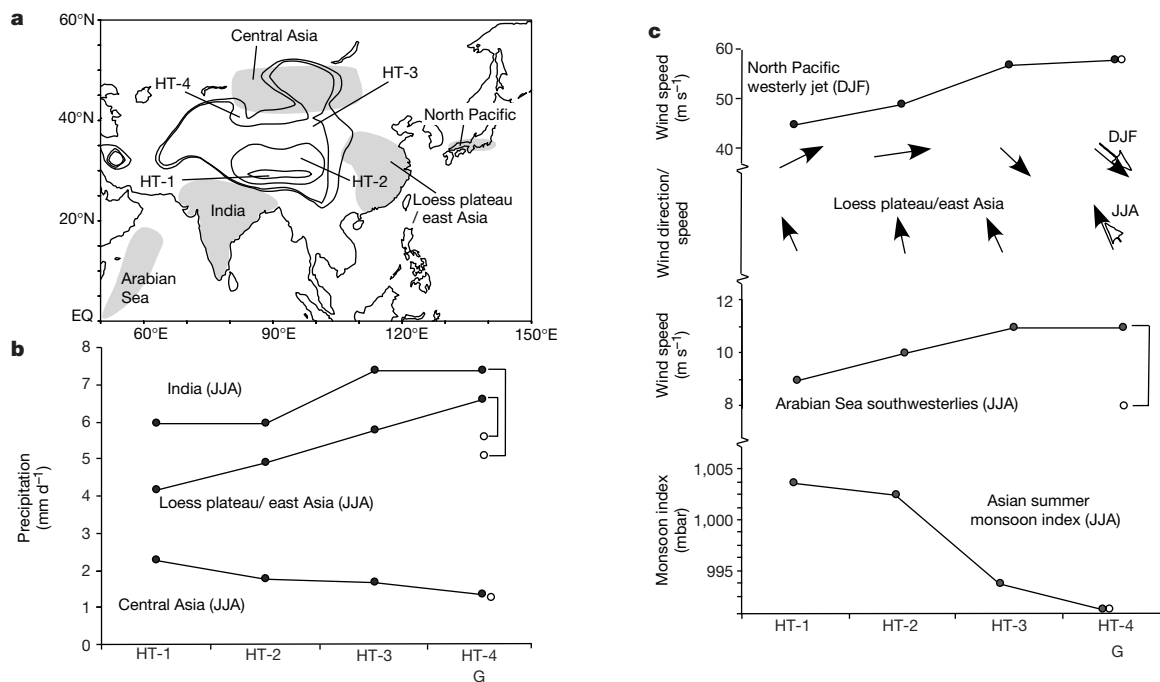


Figure 3 Climate indices from an experiment with four idealized stages of Himalaya–Tibetan plateau elevation (HT-1 to HT-4) and one glacial maximum stage (G) made with the NCAR climate model CCM3. **a**, Areas (in grey) for which climate indices are summarized (below), and approximate boundaries of the idealized topography stages with elevations higher than 1,000 m outlined: HT-1, small elevated region, with maximum elevation less than 1,700 m; HT-2, Himalaya and Tibetan plateau of limited north–south and east–west extent with maximum elevation 2,700 m; HT-3, Himalaya and Tibetan plateau considerably extended to the north and west with maximum elevation 5,700 m; and HT-4, modern, with extension of the plateau along the eastern and northern margins and maximum elevation 5,700 m. The elevations used in the climate model reflect a smoothing of the topography consistent with the spatial resolution of the climate model, and are significantly lower than the observed or estimated elevations. **b**, The June–July–August (JJA) precipitation for India, the Loess plateau/east Asia, and central Asia, for four simulations (HT-1 to HT-4) with progressive increase in mountain–plateau elevation and one simulation (G) with glacial-age modifications to HT-4 (lowered atmospheric CO₂

concentration, enlarged Northern Hemisphere ice sheets, lowered sea surface temperatures). The climate values for G are indicated with an open circle connected to the climate value for HT-4 by a thin vertical line. An off-line vegetation model, forced by the seasonal cycle of temperature and precipitation, indicates a transition from forest towards grasslands in response to uplift. In southern Asia, the area of savannah/steppe is 10% (HT-2), 33% (HT-4) and 50% (G). In the Loess plateau, the area of steppe/desert is 15% (HT-2), 35% (HT-4) and 35% (G). In central Asia, the area of steppe/desert is 30% (HT-2), 70% (HT-4) and 70% (G). **c**, Wind and circulation indices for the four elevation stages and the one glacial stage: westerly jet-stream winds in December–January–February (DJF) for the western North Pacific, wind direction and relative speed (length of arrow) in JJA and DJF for the Loess plateau/east Asia region (the open arrows refer to stage G), southwesterly winds in the Arabian Sea in JJA, and an index of the intensity of the large continent-scale Asian summer monsoon, JJA, given by the sea-level pressure at the centre of the monsoon circulation.

variability of the monsoon indices but relatively small trends compared to the subsequent period. The period from about 3.6 to 2.6 Myr ago contains the most-sustained and simultaneous intensification of both summer and winter monsoons on the Loess plateau (as indicated by magnetic susceptibility, Rb/Sr, coarse grain-size fraction, and Al flux indices), as well as the most-sustained increase of aeolian flux to the North Pacific. This simultaneous intensification of both summer and winter monsoons is difficult to explain, because the rapid increase in the volume of continental ice sheets during this same period—as inferred from the marine oxygen isotope record²⁰ (Fig. 4)—implies a shift of the climate towards more glacial conditions. Based on climate-model simulations of glacial conditions, we would expect a weakening of the summer monsoon and a strengthening of the winter monsoon²¹. Therefore, we attribute the simultaneous strengthening of both summer and winter monsoons on the Loess plateau to additional, incremental plateau uplift or extension (see below). Enhanced uplift along the northern and eastern margins of the plateau after 3.6 Myr ago is inferred from widely distributed conglomerates and increased sediment flux after 3.6 Myr ago in the west Kunlun mountains²² (Fig. 4), from conglomerates dating 3.6–2.6 Myr ago in the Linxia basin²³, from a northeastward shift in maximum sedimentation rate in basins north of the east Kunlun mountains since Pliocene times²⁴, from well-developed molasse sediments as old as 3.4 Myr in the Qaidam basin²⁴, from coarse conglomerates dating from 3.6 Myr ago at Lao Junmiao on the northern flank of the Qilian mountains (Fang, X.M., personal communication), and from indications of tectonic activity (since the Pliocene) at Haiyuan, on the eastern margin of the Tibetan plateau²⁵ (Fig. 1). The magnetic susceptibility record from the Bay of Bengal also shows a rapid increase in terrigenous influx about 3.9 Myr ago (Fig. 2a). Moreover, models of plateau formation suggest continued development of the plateau towards the north and east^{26,27}.

Our climate-model simulations show that continued uplift and expansion of the plateau along its northern and eastern margins (going from stage HT-3 to HT-4, Fig. 3) enhances both summer and

winter monsoons in the region of the Loess plateau/east Asia and continues the drying trend in central Asia, but causes little change in the general Asian summer monsoon circulation or the Indian monsoon precipitation. Overall, the model results indicate that the relatively large high-elevation area that we insert in the model in going from stage HT-2 to stage HT-3, presumably reflecting elevation changes that occurred no later than about 8 Myr ago, are sufficient to alter significantly the thermally forced circulation and establish strong continent-scale summer and winter monsoons and central Asian aridity (Fig. 3). Continued elevation increases along the northern and eastern margins, in going from stage HT-3 to stage HT-4, have a more local influence restricted mainly to central Asia and the Loess plateau/east Asia sector.

The onset of major Northern Hemisphere glaciation after 2.6 Myr ago appears to have influenced, and was perhaps influenced by, the development of the Asian monsoons. After 2.6 Myr ago, the east Asian summer monsoon, reflected by the magnetic susceptibility index, becomes more variable and at times weaker (Figs 2, 4), and the phasing between orbital forcing and Indian monsoon strength changes²⁸. In contrast, the east Asian winter monsoon, reflected in the indices of the grain-size fraction and Al flux, continues strong, and even intensifies, as does the aeolian flux to the North Pacific (Figs 2, 4), indicating sustained or intensified central Asian aridity. These changes are consistent with the climate-model simulations for glacial conditions²¹: weakened summer monsoons, but continued aridity in central Asia and strong winter monsoon north-westerly winds across eastern Asia, and strong westerlies aloft (stage G, Fig. 3). The increased atmospheric dust loading associated with central Asian aridity and strong winter winds may have helped cool global climate¹¹, and thereby contributed to the development or intensification of glaciation.

We have ignored other possible influences on Late Miocene–Pliocene climates such as uplift elsewhere²⁹, changes in ocean gateways³⁰, decreases in atmospheric CO₂ concentrations due to increased weathering or carbon burial²⁹, and changes in land/ocean configuration³¹. Nevertheless, the terrestrial records from the Loess

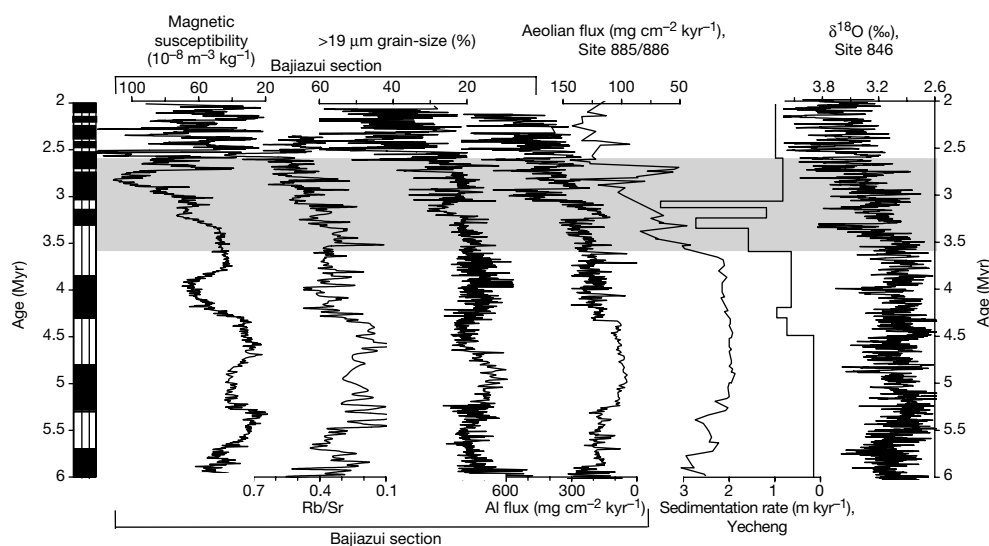


Figure 4 Terrestrial and marine records dating from 6 to about 2 Myr ago from China and the North Pacific, and indicating changes in Asian climate and global-scale glaciation. The shaded time interval between 3.6 and 2.6 Myr ago indicates the period of sustained strengthening of summer and winter monsoons on the Loess plateau. The time series are: magnetic susceptibility, Rb/Sr ratio, >19 μm grain size, and Al flux (Al content multiplied by sedimentation rate and the mean dust density of 2.5 g cm⁻³) from the Bajiazui section on the Loess plateau (Fig. 1); aeolian dust flux from North Pacific ODP sites 885 and 886 (Fig. 1)¹¹; sedimentation rate at Yecheng, north of the West Kunlun mountains²²; and δ¹⁸O from ODP core 846 in the eastern equatorial Pacific²⁰. The chronology of monsoon proxy

sequences of the Bajiazui section was obtained by interpolation with a sedimentation-rate model using >19 μm grain-size fraction, based on the magnetic stratigraphy⁶ and calibrated with polarity boundary ages²⁰. The palaeomagnetic results have also been confirmed by analysis of duplicate samples at the Geomagnetism Laboratory, University of Liverpool. Sampling resolution is 5–10 kyr. Sedimentation rate of the debris sequence at Yecheng is calculated based on its original thickness and polarity boundary ages. In the simplified stratigraphy column, the vertically hatched and solid black areas represent respectively loess (or loess-like) sediment and palaeosols.

plateau and the marine records from the Indian Ocean, interpreted with the aid of climate-model simulations that take into account both uplift and lateral extension of the Tibetan plateau, support and extend earlier conclusions^{11,17} concerning the nature and probable causes of the multi-stage evolution of Asian climates. □

Received 8 January; accepted 9 March 2001.

1. Kutzbach J. E., Prell, W. L. & Ruddiman W. F. Sensitivity of Eurasian climate to surface uplift of the Tibetan Plateau. *J. Geol.* **101**, 177–190 (1993).
2. Kutzbach J. E., Ruddiman, W. F. & Prell, W. L. in *Tectonic Uplift and Climate Change* (ed. Ruddiman, W. F.) 149–170 (Plenum, New York, 1997).
3. Broccoli, A. J. & Manabe, S. The effects of orography on midlatitude Northern Hemisphere dry climates. *J. Clim.* **5**, 1181–1201 (1992).
4. Molnar, P., England, P. & Martiodi, J. Mantle dynamics, uplift of the Tibetan Plateau and the Indian monsoon development. *Rev. Geophys.* **34**, 357–396 (1993).
5. Harrison, T. M., Copeland, P., Kidd, W. S. F. & Yin, A. Raising Tibet. *Science* **255**, 1663–1670 (1992).
6. Sun, D. H., Liu, T. S., Chen, M. Y. & Shaw, J. Magnetostratigraphy and paleoclimate of Red Clay sequences from the Chinese Loess Plateau. *Sci. China D*. **40**, 337–343 (1997).
7. Sun, D. H., An, Z. S., Shaw, J., Bloemendal, J. & Sun, Y. B. Magnetostratigraphy and palaeoclimatic significance of Late Tertiary aeolian sequences in the Chinese Loess Plateau. *Geophys. J. Int.* **134**, 207–212 (1998).
8. Prell, W. L., Murray, D. W., Clemens, S. C. & Anderson, D. M. in *Synthesis of Results from Scientific Drilling in the Indian Ocean* (eds Duncan, R. A. *et al.*) 447–469 (Geophysical Monograph Series 70, American Geophysical Union, Washington DC, 1992).
9. Prell, W. L. & Kutzbach, J. E. in *Tectonic Uplift and Climate Change* (ed. Ruddiman, W. F.) 172–203 (Plenum, New York, 1997).
10. Kroon, D., Steens, T. N. F. & Troelstra, S. R. Onset of monsoonal related upwelling in the western Arabian Sea. *Proc. ODP Sci. Res.* **117**, 257–263 (1991).
11. Rea, D. K., Snoeck, H. & Joseph, L. H. Late Cenozoic eolian deposition in the North Pacific: Asian drying, Tibetan uplift, and cooling of the Northern Hemisphere. *Paleoceanography* **13**, 215–224 (1998).
12. Quade, J., Cerling, T. E. & Bowman, J. R. Development of Asian monsoon revealed by marked ecological shift in the latest Miocene of northern Pakistan. *Nature* **342**, 163–166 (1989).
13. Cerling, T. E. *et al.* Global vegetation change through the Miocene/Pliocene boundary. *Nature* **389**, 153–158 (1997).
14. Ma, Y. Z., Li, J. J. & Fang, X. M. Pollen assemblage in 30.6–5.0 Ma redbeds of Linxia region and climate evolution. *Chinese Sci. Bull.* **43**, 301–304 (1998).
15. Porter, S. C. & An, Z. S. Correlation between climate events in the North Atlantic and China during the last glaciation. *Nature* **375**, 305–308 (1995).
16. Kukla, G. & An, Z. S. Loess stratigraphy in central China. *Paleogeogr. Paleoclimatol. Paleocool.* **72**, 203–225 (1989).
17. An, Z. S. *et al.* Eolian evidence from the Chinese Loess Plateau: the onset of the late Cenozoic Great Glaciation in the Northern Hemisphere and Qinghai-Xizang Plateau uplift forcing. *Sci. China D* **42**, 258–271 (1999).
18. Maher, B. A. Characterization of soils by mineral magnetic measurements. *Phys. Earth Planet. Inter.* **42**, 76–92 (1986).
19. Chen, J., An, Z. S. & Head, J. Variation of Rb/Sr ratios in the loess-paleosol sequences of central China during the last 130,000 years and their implications for monsoon paleoclimatology. *Quat. Res.* **51**, 215–219 (1999).
20. Shackleton, N. J., Hall, M. A. & Pate, D. Pliocene stable isotope stratigraphy of site 846. *Proc. ODP Sci. Res.* **138**, 337–355 (1995).
21. Prell, W. L. & Kutzbach, J. E. Sensitivity of the Indian monsoon to forcing parameters and implications for its evolution. *Nature* **360**, 647–652 (1992).
22. Zheng, H., Powell, C., An, Z., Zhou, J. & Dong, G. Pliocene uplift of the northern Tibetan Plateau. *Geology* **28**, 715–718 (2000).
23. Li, J. *et al.* Late Cenozoic magnetostratigraphy (11–0 Ma) of the Dongshanding and Wangjiashan section in the Longzhong Basin, western China. *Geol. Mijnbouw* **76**, 121–134 (1997).
24. Metivier, F., Gaudemer, Y., Tapponnier, P. & Meyer, B. Northeastward growth of the Tibet plateau deduced from balanced reconstruction of two depositional areas: the Qaidam and Hexi Corridor basins, China. *Tectonics* **17**, 823–842 (1998).
25. Burchfiel, B. C. *et al.* Geology of the Haiyuan fault zone, Ningxia-Hui Autonomous region, China, and its relation to the evolution of the northeastern margin of the Tibetan Plateau. *Tectonics* **10**, 1091–1110 (1991).
26. Royden, L. H. *et al.* Surface deformation and lower crustal flow in Eastern Tibet. *Science* **276**, 788–790 (1997).
27. England, P. & Houseman, G. Finite strain calculations of continental deformation. Comparison with India-Asia collision. *J. Geophys. Res.* **91**, 3664–3676 (1986).
28. Clemens, S., Murray, D. W. & Prell, W. L. Nonstationary phase of the Plio-Pleistocene Asian monsoon. *Science* **274**, 943–948 (1996).
29. Raymo, M. E., Ruddiman, W. F. & Froelich, P. N. Influence of late Cenozoic mountain building on ocean geochemical cycles. *Geology* **16**, 649–653 (1988).
30. Haug, G. H. & Tiedemann, R. Effect of the formation of the Isthmus of Panama on Atlantic Ocean thermohaline circulation. *Nature* **393**, 673–676 (1998).
31. Ramstein, G., Fluteau, F., Besse, J. & Joussaume, S. Effect of orogeny, plate motion and land-sea distribution on Eurasian climate change over the past 30 million years. *Nature* **386**, 788–795 (1997).

Acknowledgements

The model simulations used climate models and computer resources provided by the National Center for Atmospheric Research in Boulder, Colorado. This work was supported by the Chinese Academy of Sciences, the Chinese Ministry of Science and Technology, and the Chinese National Science Foundation, and by grants to the University of Wisconsin and Brown University from the US National Science Foundation.

Correspondence and requests for materials should be addressed to J.E.K. (e-mail: jek@facstaff.wisc.edu).

Phosphorus limitation of nitrogen fixation by *Trichodesmium* in the central Atlantic Ocean

Sergio A. Sañudo-Wilhelmy*, Adam B. Kustka*, Christopher J. Gobler†, David A. Hutchins‡, Min Yang*, Kamazima Lwiza*, James Burns§, Douglas G. Capone§, John A. Raven|| & Edward J. Carpenter¶

* Marine Sciences Research Center, State University of New York, Stony Brook, New York 11794-5000, USA

† Southampton College, Natural Science Division, Long Island University, Southampton, New York 11968, USA

‡ College of Marine Studies, University of Delaware, Lewes, Delaware 19958, USA

§ Wrigley Institute for Environmental Studies and Department of Biological Sciences, University of Southern California, Los Angeles, California 90089, USA

|| Division of Environmental and Applied Biology, School of Life Sciences, University of Dundee, Dundee DD1 4HN, UK

¶ Romberg Tiburon Center, San Francisco State University, Tiburon, California 94920, USA

Marine fixation of atmospheric nitrogen is believed to be an important source of biologically useful nitrogen to ocean surface waters¹, stimulating productivity of phytoplankton and so influencing the global carbon cycle². The majority of nitrogen fixation in tropical waters is carried out by the marine cyanobacterium *Trichodesmium*³, which supplies more than half of the new nitrogen used for primary production⁴. Although the factors controlling marine nitrogen fixation remain poorly understood, it has been thought that nitrogen fixation is limited by iron availability in the ocean^{2,5}. This was inferred from the high iron requirement estimated for growth of nitrogen fixing organisms⁶ and the higher apparent densities of *Trichodesmium* where aeolian iron inputs are plentiful⁷. Here we report that nitrogen fixation rates in the central Atlantic appear to be independent of both dissolved iron levels in sea water and iron content in *Trichodesmium* colonies. Nitrogen fixation was, instead, highly correlated to the phosphorus content of *Trichodesmium* and was enhanced at higher irradiance. Furthermore, our calculations suggest that the structural iron requirement for the growth of nitrogen-fixing organisms is much lower than previously calculated⁶. Although iron deficiency could still potentially limit growth of nitrogen-fixing organisms in regions of low iron availability—for example, in the subtropical North Pacific Ocean—our observations suggest that marine nitrogen fixation is not solely regulated by iron supply.

We collected surface water samples and colonies of *Trichodesmium* spp. using trace-metal clean methods along two transects in the tropical (0–6° N latitude; 50–28° W longitude) and subtropical (10–16° N; 30–55° W) Atlantic Ocean in April 1996, and analysed them for C, N, P and Fe content. We also measured N₂ fixation rates of colonies (Methods).

Strong spatial gradients in the N₂-fixing diazotrophic activity were observed along the tropical and subtropical transects. Cell C specific N₂ fixation in the subtropical northern transect (median was 152 μmol N per mol C per h) was four times higher than in the tropical transect (median was 38 μmol N per mol C per h) (Fig. 1a). *Trichodesmium* biomass (Fig. 1b) was also seven times higher in the northern subtropical transect (subtropical median was 1.44 per mg chl *a* per m²; tropical median was 0.20 per mg chl *a* per m²).

In contrast to N₂ fixation, dissolved Fe concentrations in surface waters of the sub-tropical (median was 0.77 nM) and tropical (median was 0.95 nM) Atlantic were relatively constant (Fig. 1c). Similarly, levels of Fe in field-collected *Trichodesmium* colonies